

Supporting information

Extendable nickel complex tapes that reach NIR absorptions

Hassib Audi, Zhongrui Chen, Azzam Charaf-Eddin, Anthony D'Aléo, Gabriel Canard, Denis Jacquemin, Olivier Siri**

CINaM, UMR 7325 CNRS, Aix-Marseille Université, Campus de Luminy, case 913, F-13288 Marseille cedex 09, France.

*Correspondence to: olivier.siri@univ-amu.fr, Denis.Jacquemin@univ-nantes.fr

1. General informations	S2
2. Synthesis	S2
3. NMR studies	S8
4. Electronic absorption properties	S10
5. Electrochemical study	S12
6. Quantum mechanical calculations	S12
7. References	S16

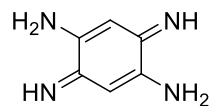
1. General Informations

Analytical-grade reagents were obtained from commercial suppliers and were used directly without further purification. ^1H NMR and ^{13}C NMR spectra in solution were recorded on a AC250 Bruker spectrometer operating at 250 MHz and 62 MHz, respectively. Chemical shifts are reported in delta (δ) units, expressed in parts per million (ppm) using the residual protonated solvent as an internal standard ($(\text{CD}_3)_2\text{SO}$) 2.50 ppm; CDCl_3 7.26 ppm). The multiplicity of signals is designated by the following abbreviations: s, singlet; br s, broad singlet. High-resolution mass spectrometry (HRMS) was performed on a Q-STAR Elite.

2. Synthesis

3,6-diimino-1,4-cyclohexadiene-1,4-diamine (2)

The commercially available tetraaminobenzene tetrahydrochloride ($m = 1.00$ g, 3.52 mmol) was placed in MeOH ($v = 150$ mL). Then Cs_2CO_3 ($m = 4.58$ g, 14.08 mmol) was added. The solution was then stirred at room temperature for 30 min and the resulting precipitate was isolated by filtration and dried under vacuum. Product **2** was obtained as a brown solid in 79% yield ($m = 0.380$ g, 2.79 mmol).



^1H NMR (250 MHz, $(\text{CD}_3)_2\text{SO}$): $\delta = 5.50$ (s, 2H), 5.79 (br s, 4H), 9.34 (s, 2H); ^{13}C NMR (62 MHz, $(\text{CD}_3)_2\text{SO}$): $\delta = 96.63, 146.04, 162.62$; ^{13}C solid NMR (100 MHz): $\delta = 99.35, 147.30, 165.15$; ^{15}N solid NMR (40 MHz): $\delta = -316.90, -121.21$; HRMS (ESI) calculated for $\text{C}_6\text{H}_8\text{N}_4$ $m/z = 137.0822$ $[\text{M}+\text{H}]^+$, found: 137.0820; UV-visible (CH_2Cl_2) λ (ϵ $\text{mol}^{-1}\cdot\text{L}\cdot\text{cm}^{-1}$): 317 nm (13 700).

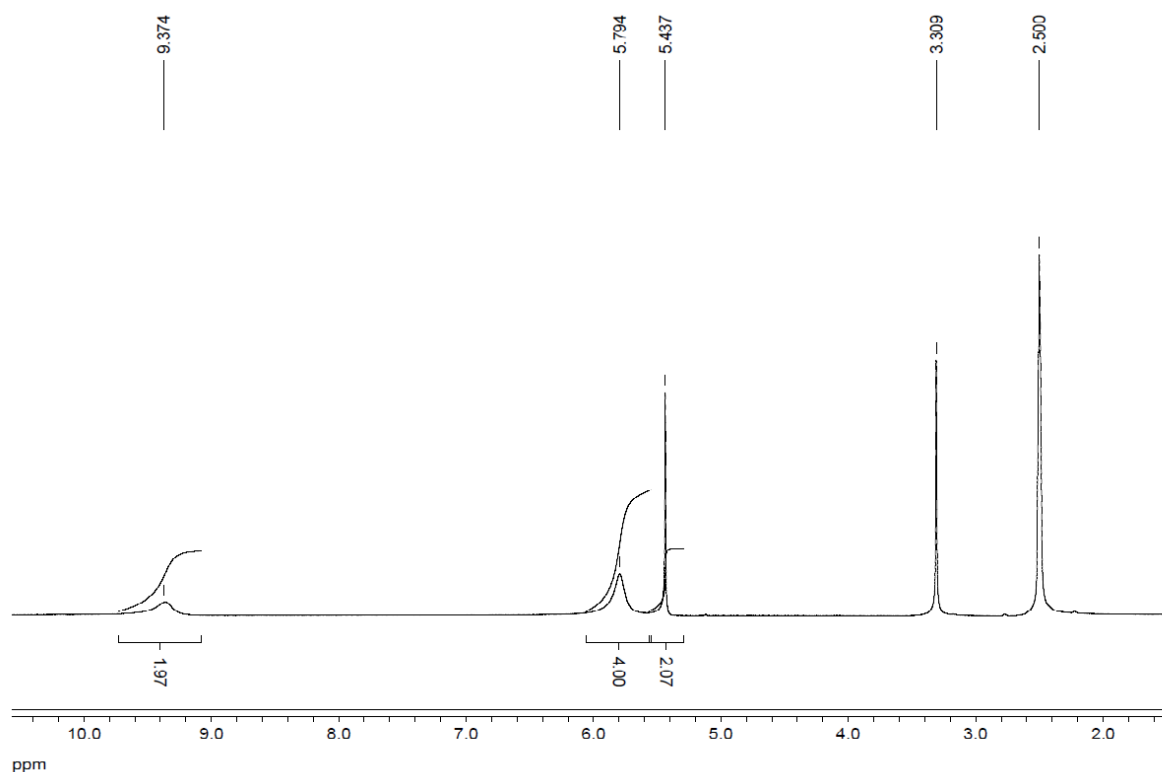


Figure S1. ^1H NMR spectrum of **2** in DMSO- d_6 at rt (250 MHz)

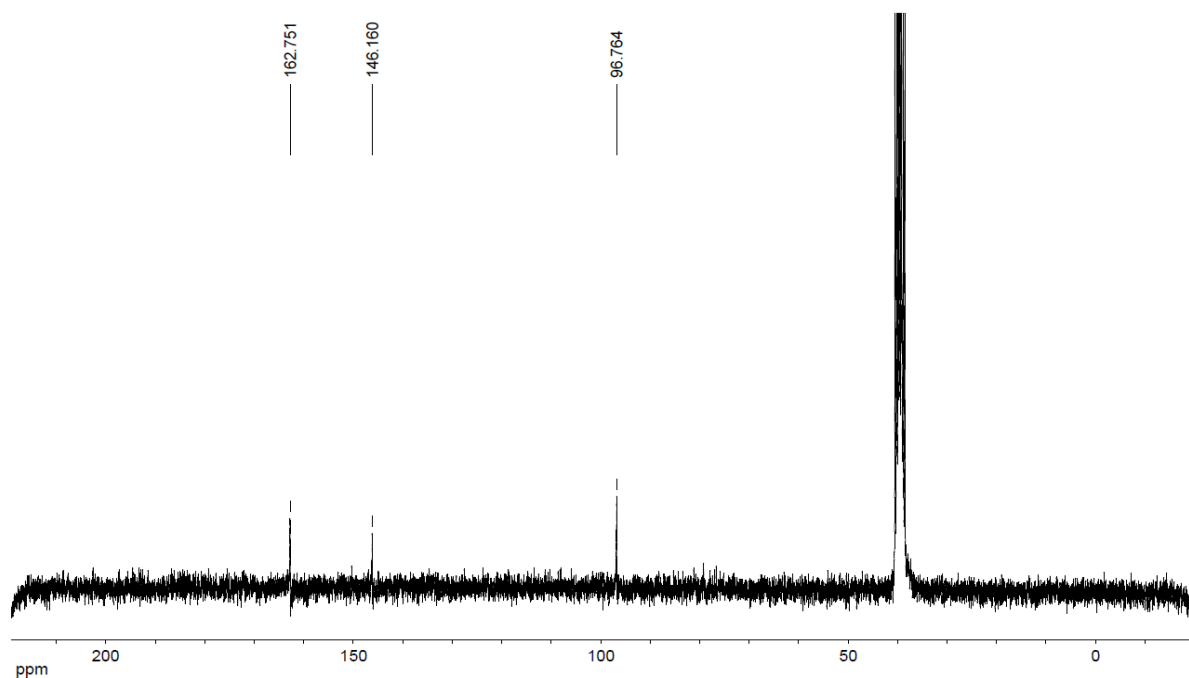
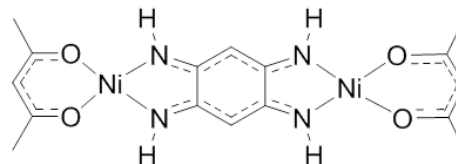


Figure S2. ^{13}C NMR spectrum of **2** in DMSO-d_6 at rt (62 MHz)

$[(\text{acac})\text{Ni}\{\mu\text{-C}_6\text{H}_2(=\text{NH})_4\}\text{Ni}(\text{acac})]$ (7**)**

To a suspension of **2** ($m = 25$ mg, 0.18 mmol) in toluene ($v = 5$ mL) was added $\text{Ni}(\text{acac})_2$ ($m = 94$ mg, 0.36 mmol). The solution was stirred at room temperature for 2h and the resulting precipitate was then isolated by filtration. The solid was recrystallized in toluene to afford the binuclear complex **7** as a green solid ($m = 46$ mg, 54% yield).



^1H NMR (250 MHz, CDCl_3): $\delta = 1.78$ (s, 12H), 3.04 (br s, 4H), 4.49 (s, 2H); 5.32 (s, 2H); ^{13}C NMR (62 MHz, CDCl_3): $\delta = 25.49, 88.29, 101.34, 168.70, 186.87$; ^{13}C solid NMR (100 MHz): δ (ppm) = 26.52, 89.04, 102.79, 169.19, 187.68; ^{15}N solid NMR (40 MHz): δ (ppm) = -283.82, -281.10, -274.39, -262.70; HRMS (ESI) calculated for $\text{C}_{16}\text{H}_{20}\text{N}_4\text{Ni}_2\text{O}_4$ $m/z = 449.0264$ $[\text{M}+\text{H}]^+$, found: 449.0191; UV-visible (CH_2Cl_2) λ (ϵ $\text{mol}^{-1}\cdot\text{L}\cdot\text{cm}^{-1}$): 475 nm (18 269), 502 nm (19 307).

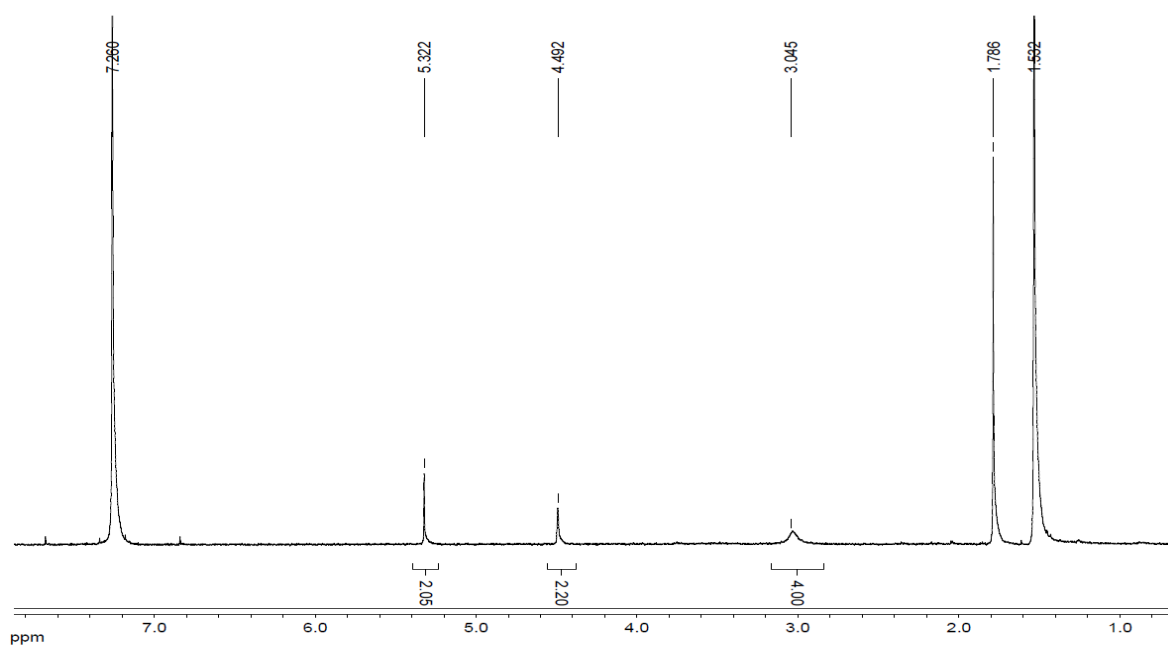


Figure S3. ^1H NMR spectrum of **7** in CDCl_3 at rt (250 MHz)

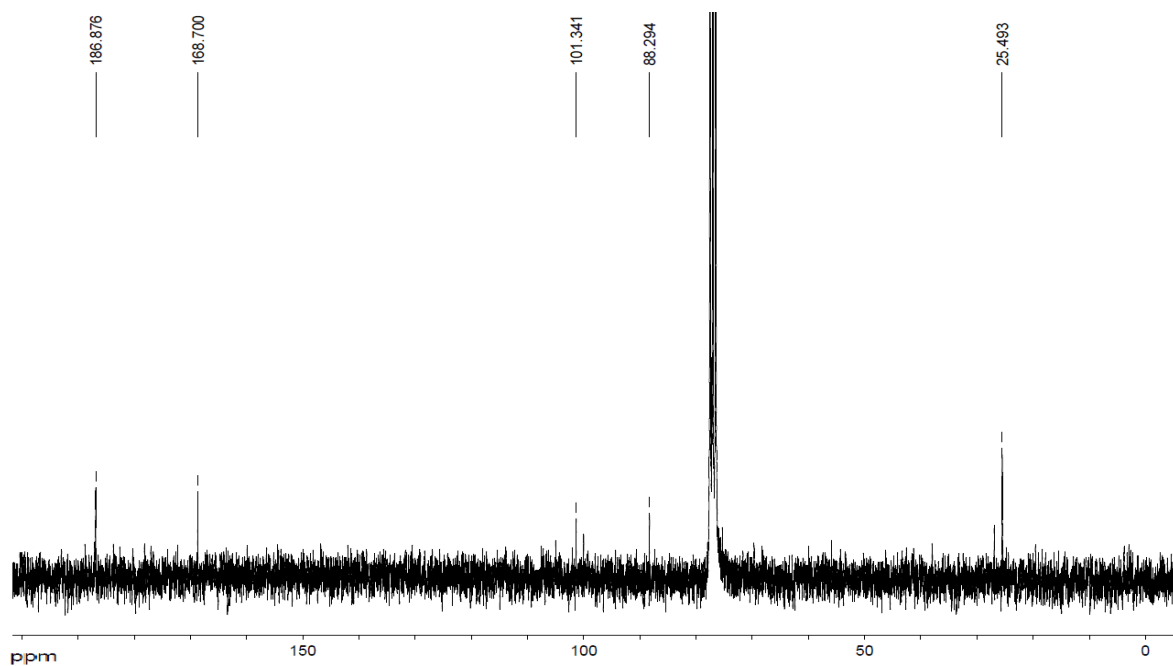
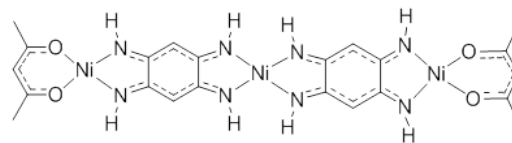


Figure S4. ^{13}C NMR spectrum of **7** in CDCl_3 at rt (62 MHz)

[(acac)Ni{ μ -C₆H₂(=NH)₄}Ni{ μ -C₆H₂(=NH)₄}Ni(acac)] (8)

To a suspension of **2** (*m* = 20 mg, 0.15 mmol) in THF (*v* = 20 mL) was added Ni(acac)₂ (*m* = 75 mg, 0.29 mmol). The reaction mixture was stirred at room temperature for 24h and the solvent was then removed by evaporation under vacuum.

The resulting solid was taken up in chloroform and the obtained precipitate was isolated by filtration to give the trinuclear complex **8** as violet solid (*m* = 72 mg, 77% yield).



¹H NMR (250 MHz, (CD₃)₂SO): δ (ppm) = 1.76 (s, 12H), 4.47 (br s, 4H), 4.63 (s, 4H); 5.08 (br s, 4H); 5.42 (s, 2H); ¹³C NMR spectrum of **8** in solution could not be recorded owing to its poor stability and solubility in DMSO; ¹³C solid NMR (100 MHz): δ (ppm) = 27.3, 29.2, 90.8, 91.6, 101.6, 169.9, 185.1, 190.0; ¹⁵N solid NMR (40 MHz): δ (ppm) = -259.2, -266.4, -270.4, -281.5; HRMS (ESI) calculated for C₂₂H₂₂N₈Ni₃O₄ *m/z* = 641.0210 [M+H]⁺, found: 641.0213; UV-visible (THF) λ (ϵ mol⁻¹.L.cm⁻¹): 576 nm (21 333), 627 nm (23 222).

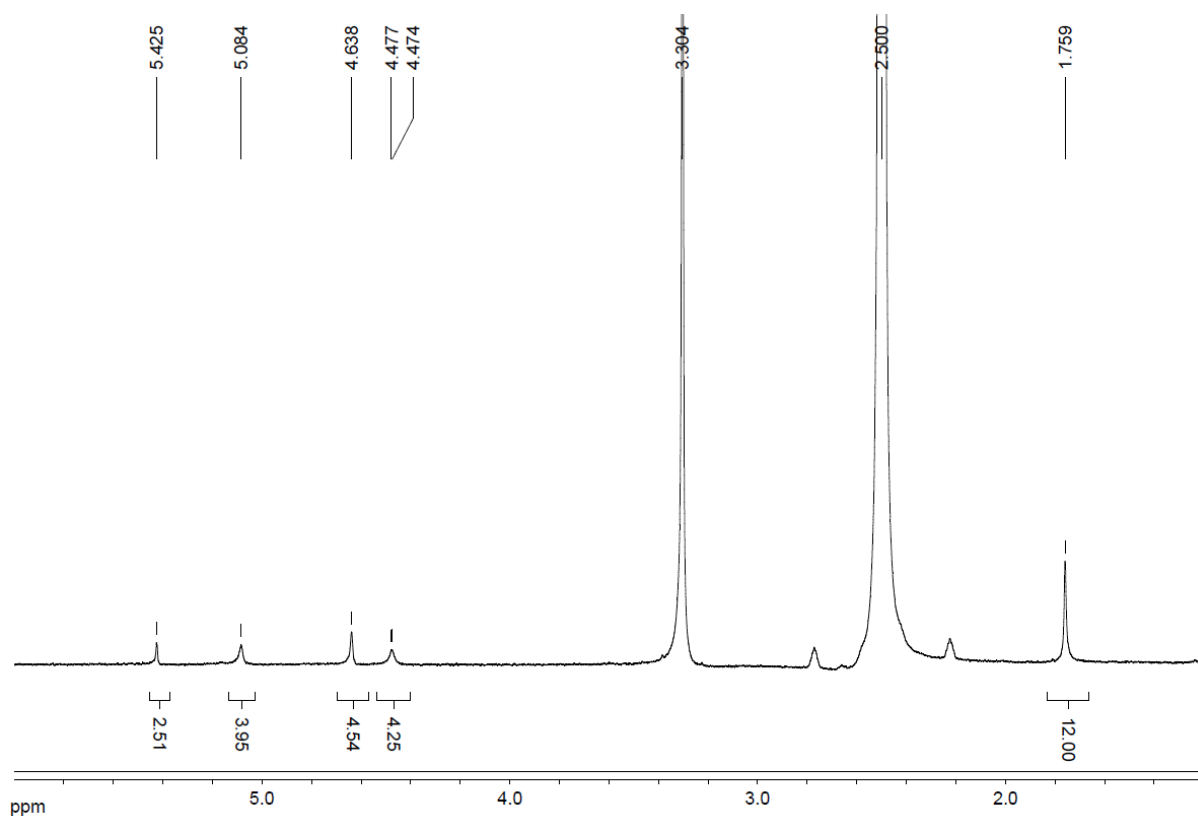


Figure S5. ¹H NMR spectrum of **8** in DMSO-d₆ at rt (250 MHz)

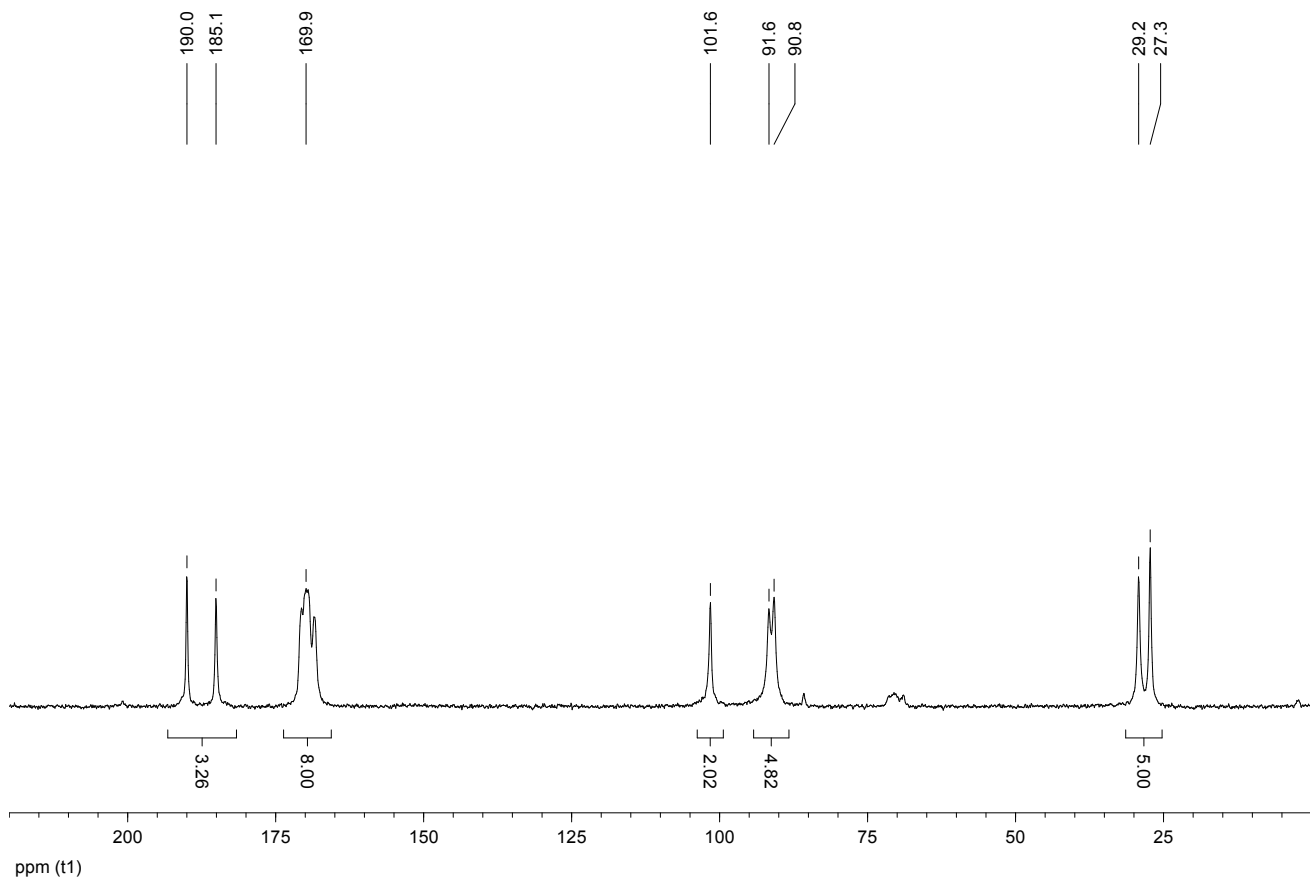


Figure S6. ^{13}C Solid-state NMR spectrum of **8** (100 MHz)

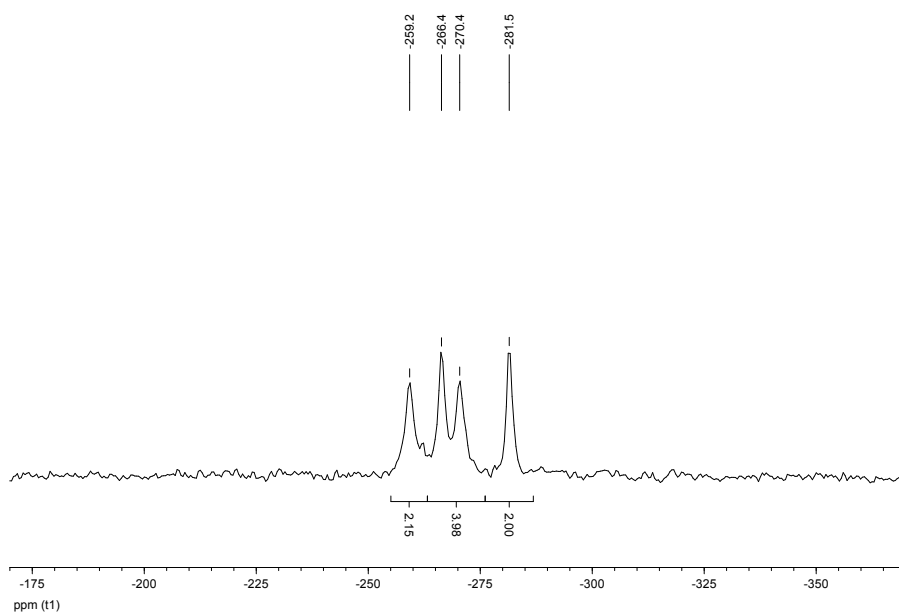
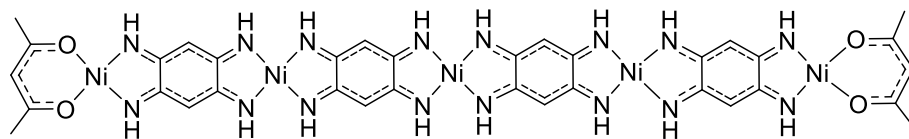


Figure S7. ^{15}N Solid-state NMR spectrum of **8** (40 MHz)

[(acac)Ni{ μ -C₆H₂(=NH)₄}Ni{ μ -C₆H₂(=NH)₄}Ni{ μ -C₆H₂(=NH)₄}Ni{ μ -C₆H₂(=NH)₄}Ni (acac)] (9)



The complex **8** (m = 30 mg; 0.047 mmol) was dissolved in DMSO (v = 15 mL) and the solution was stirred at room temperature for 24h. The resulting precipitate was isolated by filtration and washed with DMSO and CHCl₃ to give the pentanuclear complex **9** as a dark violet solid (m = 43 mg, 89% yield). ¹H and ¹³C NMR spectrum in solution could not be recorded owing to the poor solubility of **9**.

¹³C solid NMR (100 MHz): δ (ppm) = 26.85, 93.81, 102.93, 169.23, 188.29; ¹⁵N solid NMR (40 MHz): δ (ppm) = -263.93. Calculated for C₃₄H₃₈N₁₆Ni₅O₄·1CHCl₃·1DMSO: C 36.26, H 3.70, N 18.28, S 2.62, found: C 35.73, H 3.65, N 18.48, S 2.34.

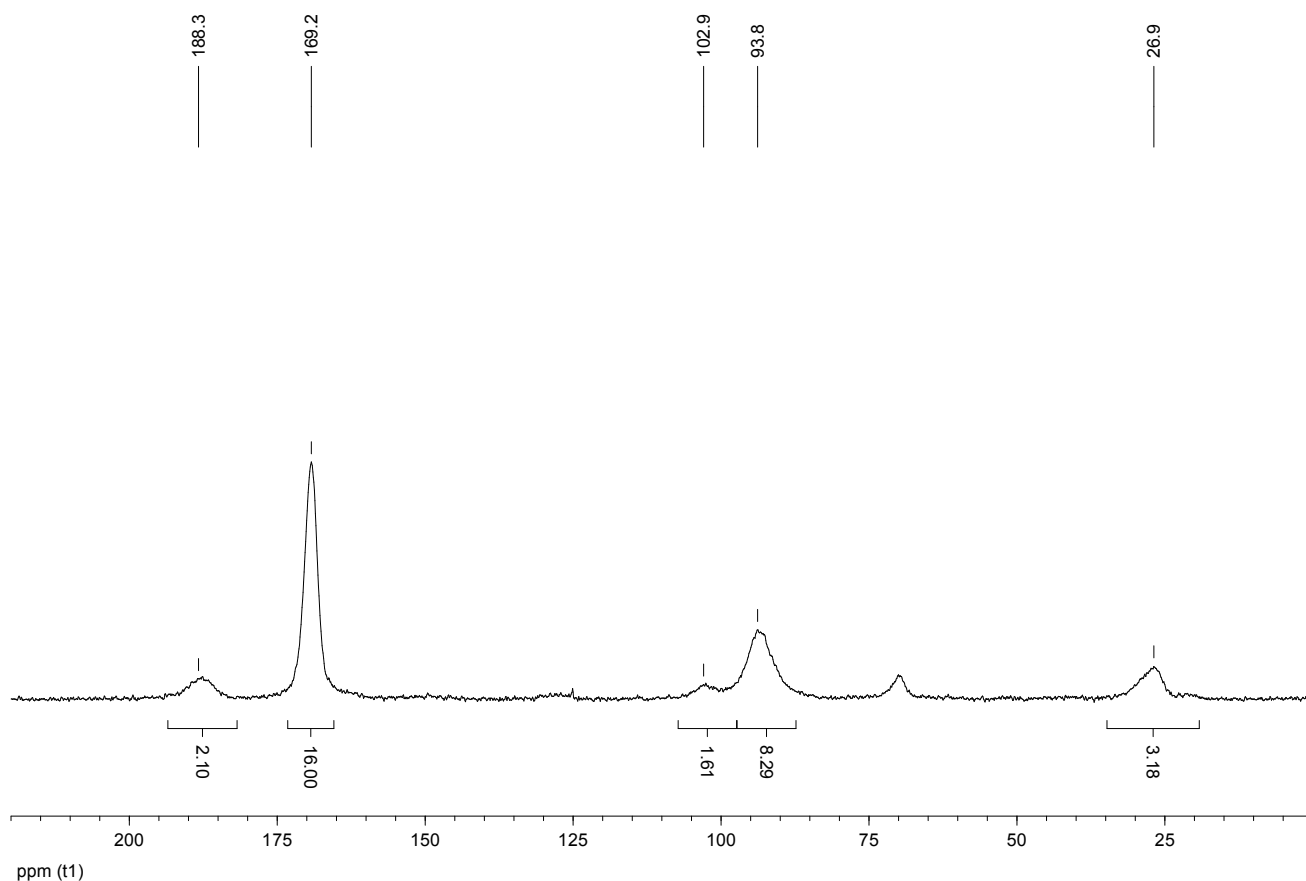


Figure S8. ¹³C Solid-state NMR spectrum of **9** (400 MHz). The C=O signals integrate for 2 instead of 4 because of its poor relaxation time.

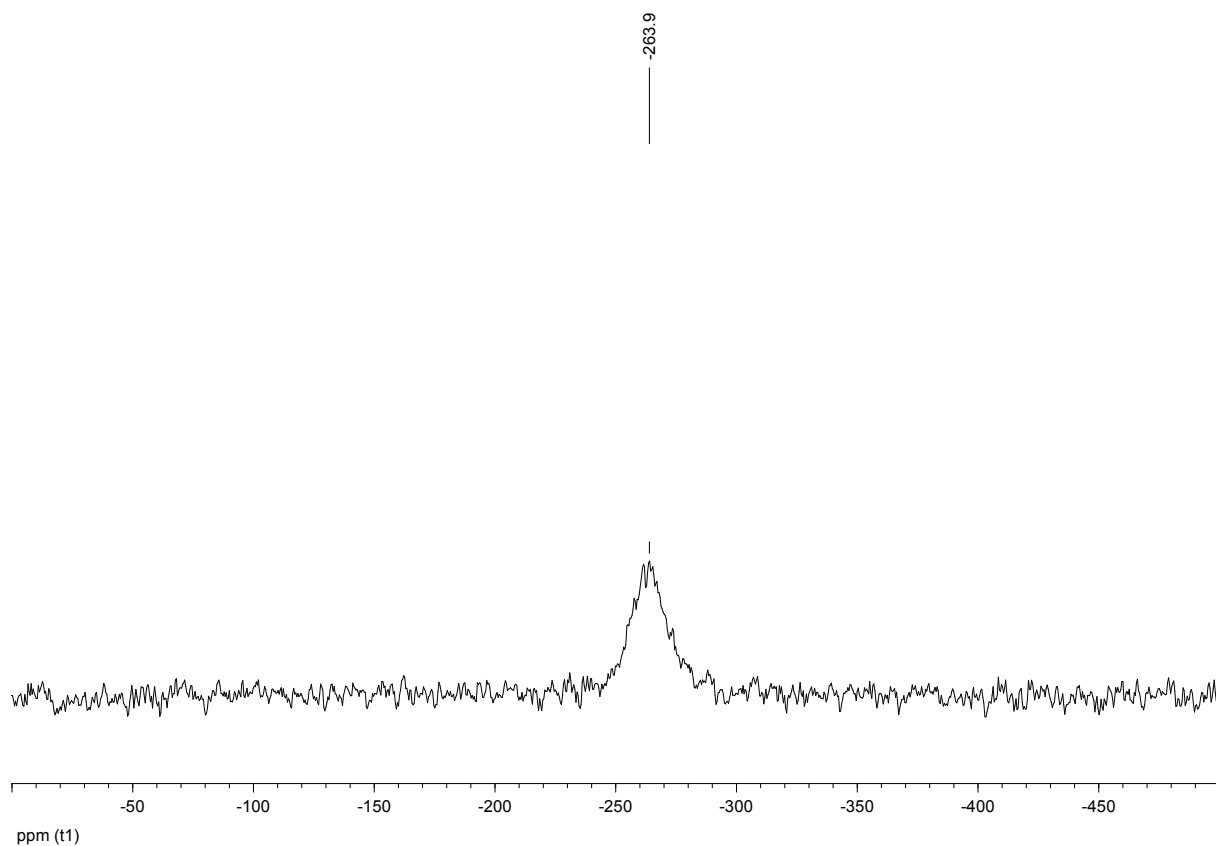


Figure S9. ^{15}N Solid-state NMR spectrum of **9** (40 MHz)

3. NMR studies

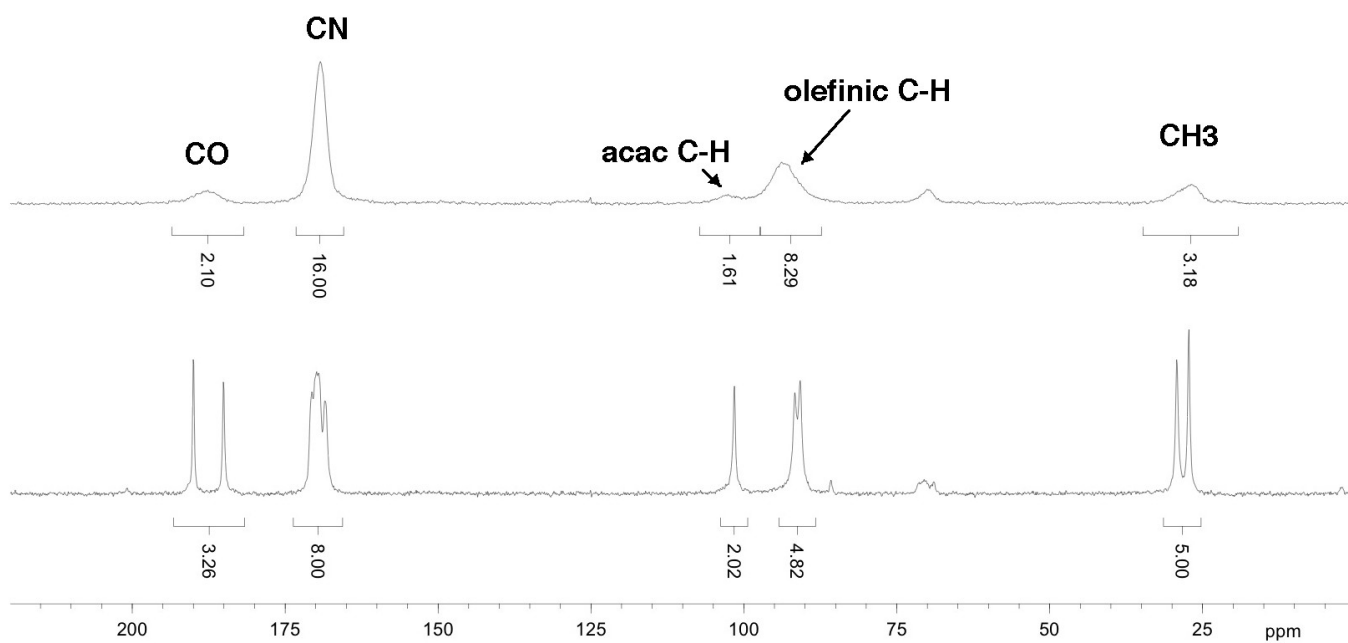


Figure S10. ^{13}C Solid-state NMR spectrum of trinuclear complex **8** (bottom) and pentanuclear complex **9** (top)

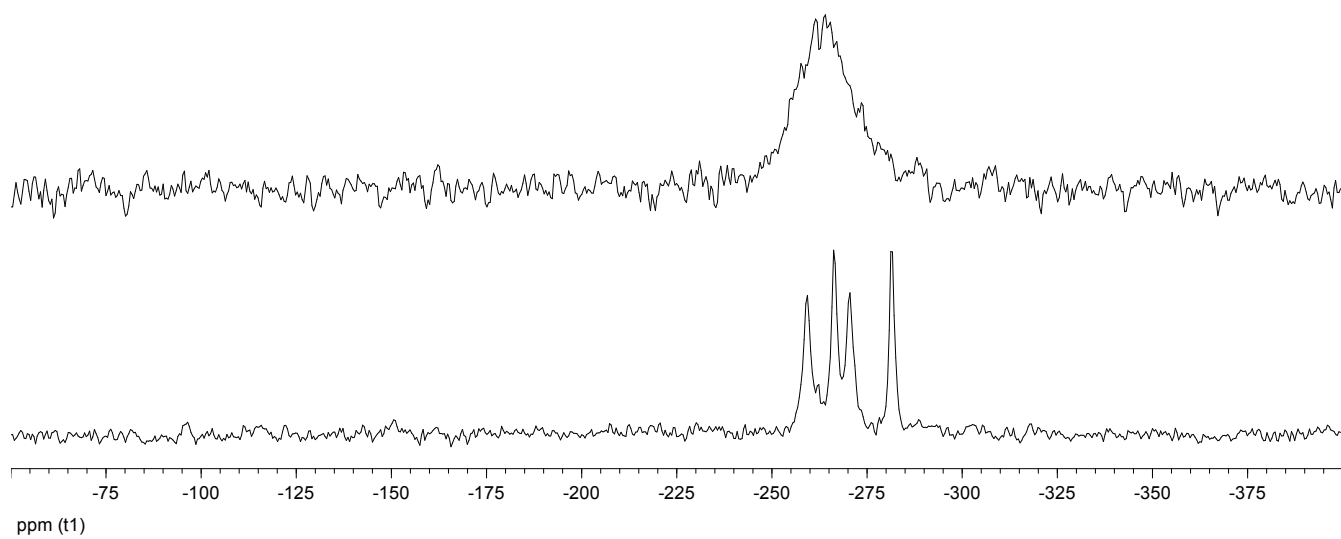


Figure S11. ^{15}N Solid-state NMR spectrum of trinuclear complex **8** (bottom) and pentanuclear complex **9** (top)

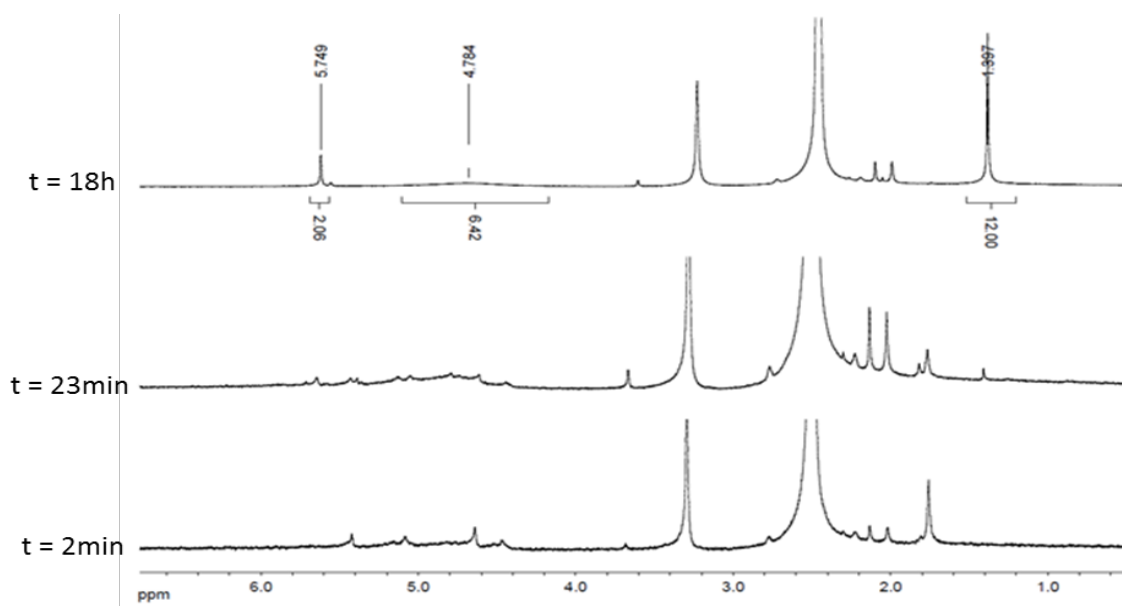


Figure S12. ^1H NMR study of the **7**→**10** conversion in DMSO-d_6 at rt (250 MHz)

4. Absorption studies

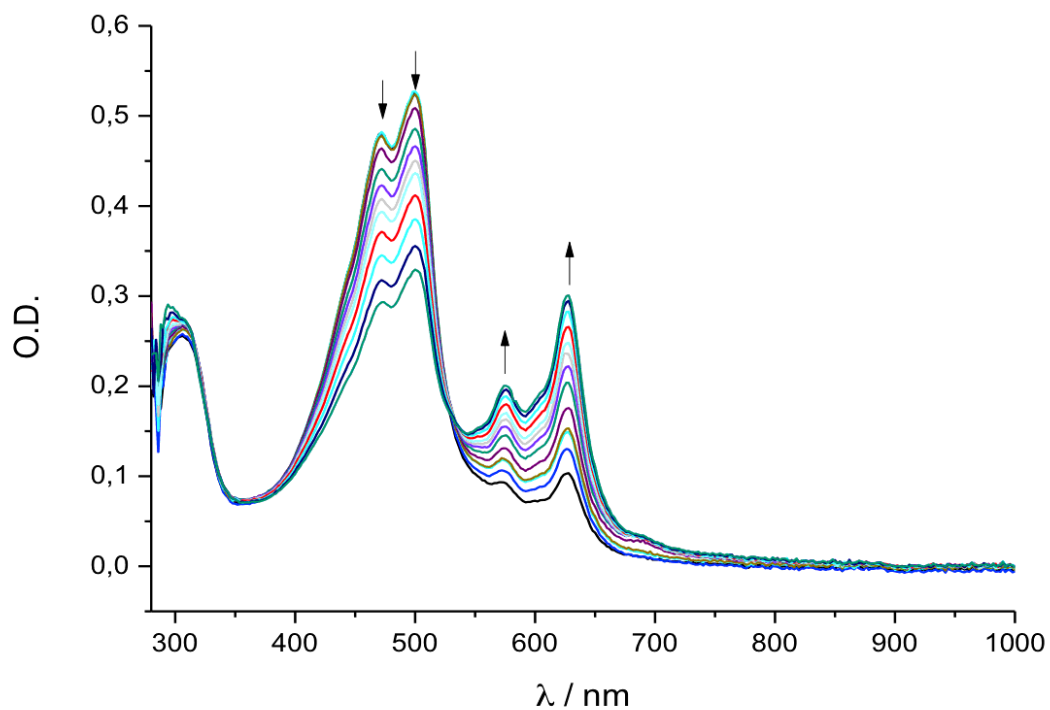


Figure S13. UV-vis-NIR spectrophotometric study of the **7**→**8** conversion in THF

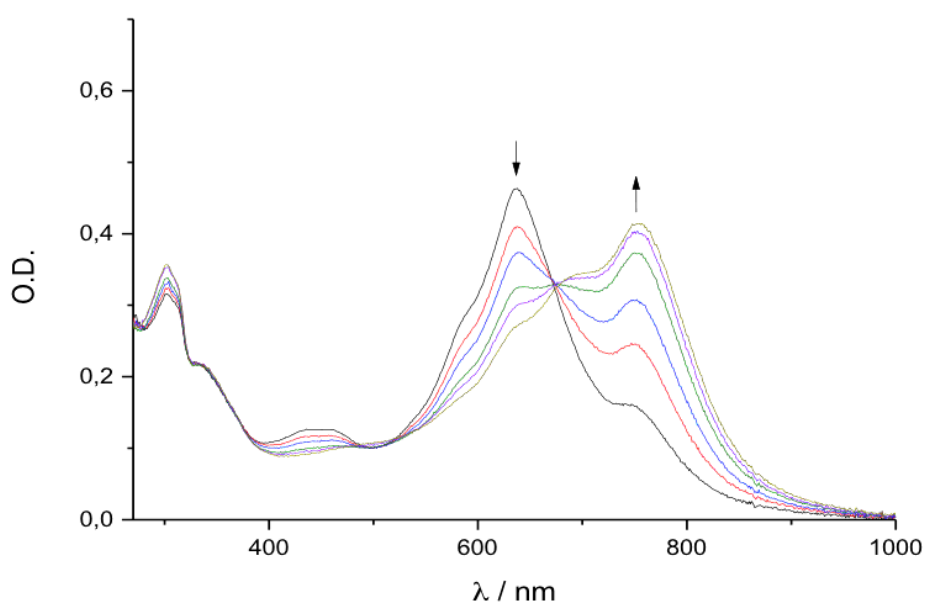


Figure S14. UV-vis-NIR spectrophotometric study of **8**→**9** conversion in DMSO.

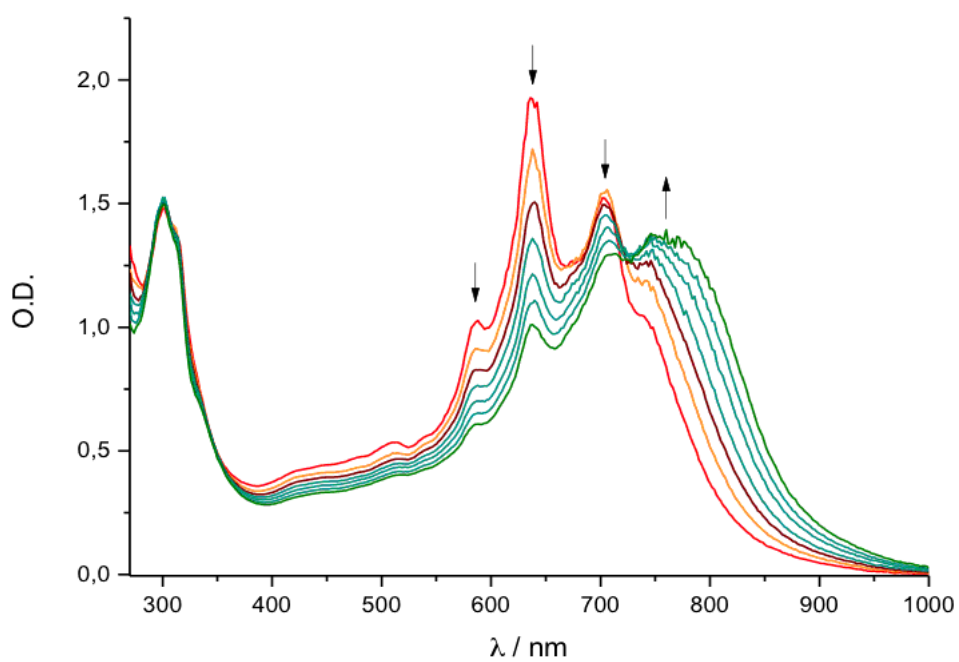
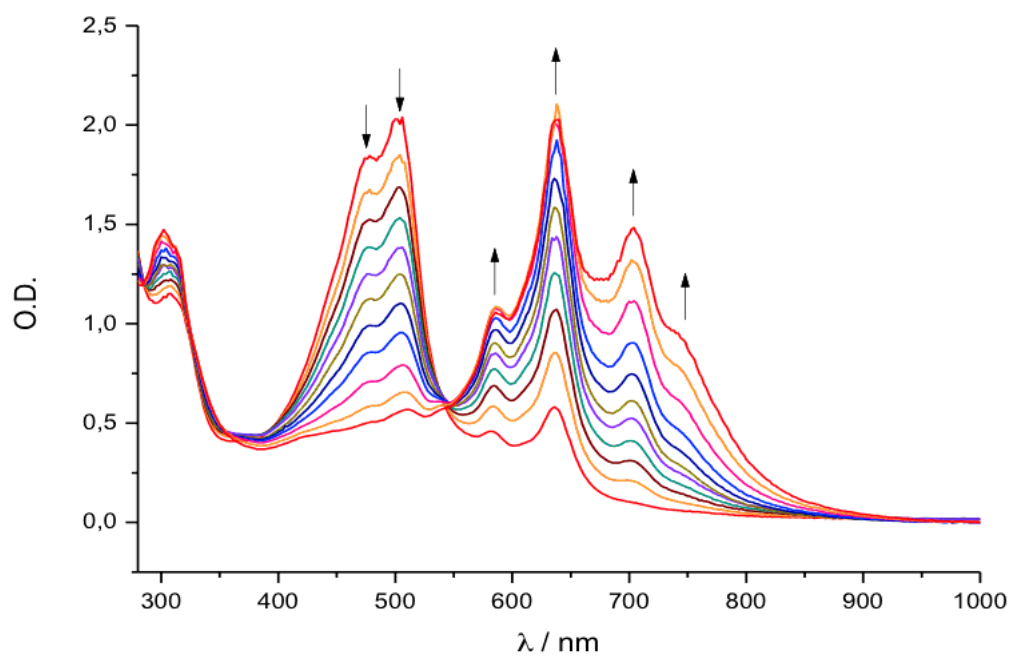


Figure S15. UV-vis-NIR spectrophotometric study: top: $7 \rightarrow 8 + 9 + 10$ conversion in DMSO, bottom: evolution of $8 \rightarrow 9 + 10$ in DMSO

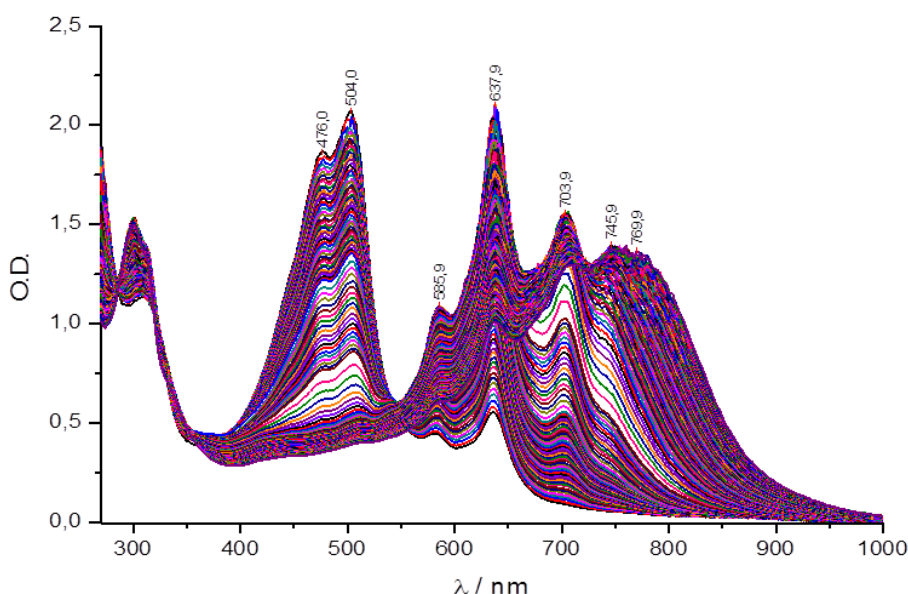


Figure S16. UV-vis-NIR spectrophotometric study of the $7 \rightarrow 8 + 9 + 10$ conversion in DMSO

5. Electrochemical study

Cyclic voltammetric (CV) data were acquired using a BAS 100 Potentiostat (Bioanalytical Systems) and a PC computer containing BAS100W software (v2.3).

A three-electrode system with a Pt working electrode (diameter 1.6 mm), a platinum counter electrode and an Ag/AgCl reference electrode. The compound was studied at 1.10^{-3} M in $\text{CD}_2\text{Cl}_2/(\text{nBu})_4\text{NPF}_6$ 0.1 M and cyclic voltammogram recorded at a scan rate of $250 \text{ mV}\cdot\text{s}^{-1}$ (Figure S17). Ferrocene was used as internal standard ($E^\circ(\text{Fc}/\text{Fc}^+) = 0.46\text{V}/\text{SCE}$). Two irreversible waves could be observed for the dinuclear compound **7** (even if the scan direction is reversed immediately after the first oxidation step).

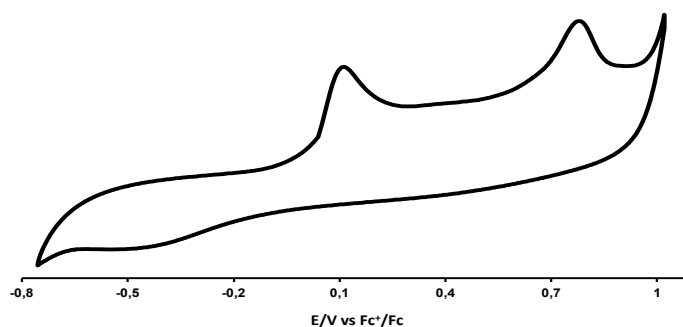


Figure S17. Cyclic voltammogram of **7** in anhydrous CH_2Cl_2 (0.1m $\text{N}(\text{nBu})_4\text{PF}_6$) at a scan rate of $100 \text{ mV}\cdot\text{s}^{-1}$

6. Quantum chemical calculations

6.1 Computational details

We have used the latest revision of the Gaussian09 program^{S1} to perform all our computations, applying default thresholds and algorithms, except when noted below. All calculations relied on the M06 hybrid exchange-correlation functional,^{S2,3} as this functional provides adequate geometrical parameters (see below) and is also known to provide accurate vertical transition energies.^{S4} We have used the 6-31G(d) atomic basis set. For all molecules, we have performed geometry optimization of the ground-state structures followed by calculations of the vibrational frequencies, confirming the absence of imaginary

frequencies. For the smallest system, we have also determined the excited-state geometries with TD-DFT using the same approach as for the ground-state. This was followed by numerical TD-DFT Hessian calculations, which allows to determine 0-0 energies^{S5} and band shapes (see below). Environmental effect have been accounted for using the well-known PCM model.^{S6} We have used both the the popular linear-response (LR) PCM approach and the corrected LR scheme (cLR).^{S7,8} The cLR scheme allows to correct the cavity polarization by account- ing for the change of electron density upon electronic transition.

Vibrationally resolved spectra have been obtained using the FCclasses program.^{S9-11} The reported spectra have been simulated using a convoluting Gaussian functions presenting a half width at half maximum (HWHM) that has been adjusted to allow accurate comparisons with experiments (0.07 eV). A maximal number of 25 overtones for each mode and 20 combination bands on each pair of modes were included in the calculation. The maximum number of integrals to be computed for each class was set to 10⁷. This is enough to reach a sufficient convergence of the FC factors. The Frank-Condon approximation has been employed as we consider strongly dipole-allowed ES.

6.2 Geometrical benchmarks

We compare in Table S1, theoretical and experimental geometries for **7**. Due to the crystal packing, the molecule departs from the D_{2h} point group, and we have considered average values in our comparisons. We have tested three exchange-correlation functionals of the M06 family. The obtained mean absolute deviations are 0.013 Å, 0.008 Å and 0.016 Å with M06-L, M06 and M06-2X, respectively with the 6-31G (d) atomic basis set. This clearly illustrates that M06 provides accurate results for the present molecule. With the larger basis set, 6-311++G(d), there is some variation of the individual bond length, especially of the metal-nitrogen and metal-oxygen distances, but the MAD are similar: 0.010 Å, 0.008 Å and 0.023 Å with M06-L, M06 and M06-2X, respectively. As we aim to treat large systems with a common approach, we selected the M06/6-31G (d) approach.

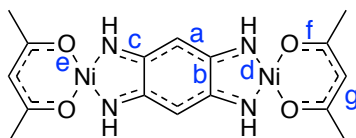


Figure S18. Convention for bond lengths in Table S1

Table S1. List of bond lengths (in Å) obtained for the molecule shown in Figure S18. Experimental data are obtained with XRD, whereas the theoretical values are gas phase results obtained with the 6-31G(d) atomic basis set. Values between brackets correspond to the 6-311++G(d,p) atomic basis set.

Parameter	Exp (min-max)	Exp (aver.)	M06-L	M06	M06-2X
a	1.379-1.394	1.388	1.397	1.395	1.397
b	1.494-1.497	1.496	(1.396)	(1.393)	(1.396)
c	1.316-1.320	1.319	1.481	1.495	1.513
d	1.839-1.867	1.853	(1.485)	(1.495)	(1.513)
e	1.845-1.851	1.849	1.329	1.319	1.314
f	1.274-1.281	1.278	(1.326)	(1.315)	(1.313)
g	1.383-1.391	1.385	1.838	1.839	1.894
			(1.868)	(1.862)	(1.914)
			1.829	1.832	1.865
			(1.863)	(1.861)	(1.892)
			1.282	1.273	1.271
			(1.276)	(1.267)	(1.266)
			1.398	1.397	1.400
			(1.399)	(1.397)	(1.402)

6.3 Vibrational analysis for 7

For the smallest system, 7, it was possible not only to perform the standard TD-DFT vertical calculations, but also to determine the excited-state geometries, vibrational frequencies and hence vibronic band shapes. The results are displayed in Figure S19 using a protocol described above, and it is clear that two peaks separated by ca. 35 nm emerge, consistently with experiment, indicating that the double maximum obtained for the monomer. The vibrational mode inducing the largest coupling is mode n°106 taking place at 1543 cm⁻¹ on the excited-state and it corresponds to a breathing mode of the central ring.

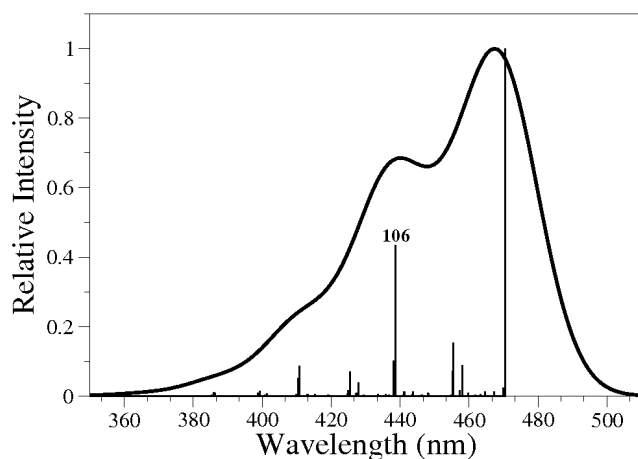


Figure S19. M06/6-31G(d) computed vibrationally resolved band shapes for 7 in THF.

6.4 Frontier orbitals

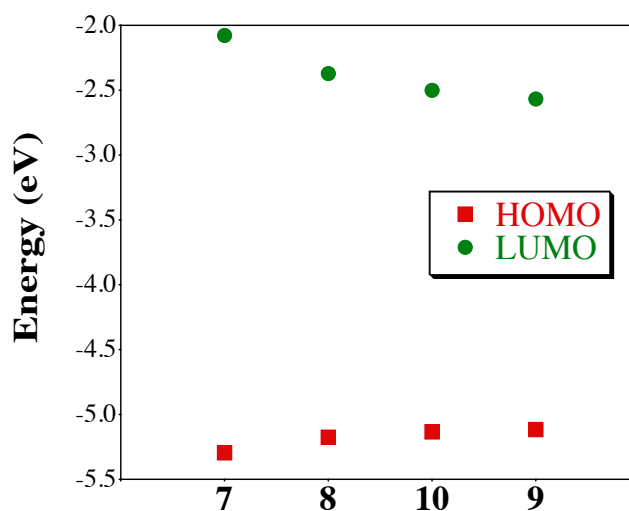


Figure S20. M06/6-31G(d) HOMO and LUMO energies computed. All values in eV

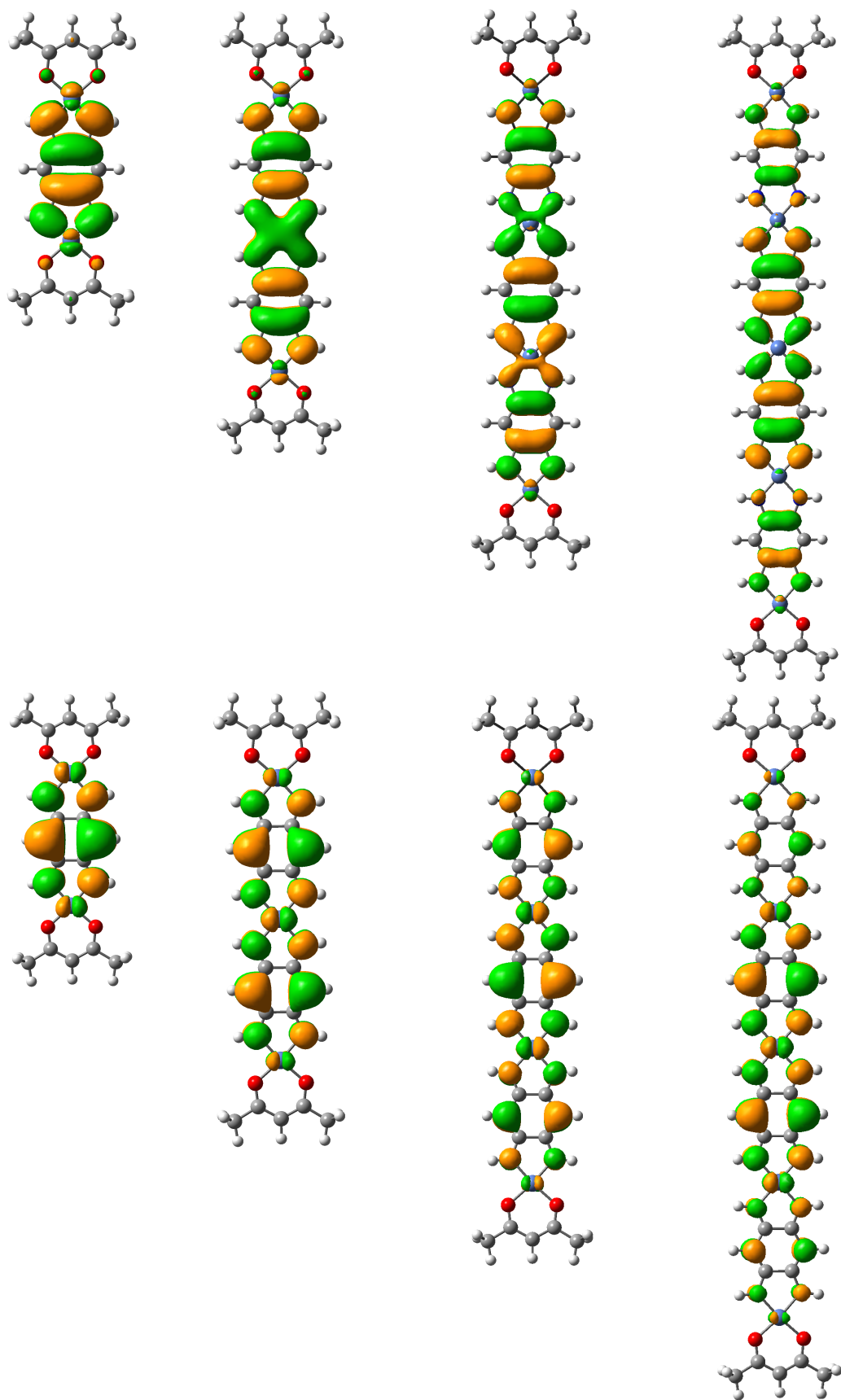


Figure S21. Sketch of the HOMO (bottom) and LUMO (top) for 7, 8, 10 and 9 (from left to right)

7. References

- S1 M. J. Frisch, G. W. Trucks, H. B. Schlegel, G. E. Scuseria, M. A. Robb, J. R. Cheeseman, G. Scalmani, V. Barone, B. Mennucci, G. A. Peters- son, H. Nakatsuji, M. Caricato, X. Li, H. P. Hratchian, A. F. Izmaylov, J. Bloino, G. Zheng, J. L. Sonnenberg, M. Hada, M. Ehara, K. Toyota, R. Fukuda, J. Hasegawa, M. Ishida, T. Nakajima, Y. Honda, O. Kitao, H. Nakai, T. Vreven, J. A. Montgomery, Jr., J. E. Peralta, F. Ogliaro, M. Bearpark, J. J. Heyd, E. Brothers, K. N. Kudin, V. N. Staroverov, R. Kobayashi, J. Normand, K. Raghavachari, A. Rendell, J. C. Burant, S. S. Iyengar, J. Tomasi, M. Cossi, N. Rega, J. M. Millam, M. Klene, J. E. Knox, J. B. Cross, V. Bakken, C. Adamo, J. Jaramillo, R. Gomperts, R. E. Stratmann, O. Yazyev, A. J. Austin, R. Cammi, C. Pomelli, J. W. Ochterski, R. L. Martin, K. Morokuma, V. G. Zakrzewski, G. A. Voth, P. Salvador, J. J. Dannenberg, S. Dapprich, A. D. Daniels, O. Farkas, J. B. Foresman, J. V. Ortiz, J. Cioslowski and D. J. Fox, *Gaussian 09 Revision D.01*, 2009, Gaussian Inc. Wallingford CT.
- S2 Y. Zhao and D. G. Truhlar, *Acc. Chem. Res.*, 2008, **41**, 157–167.
- S3 Y. Zhao and D. G. Truhlar, *Theor. Chem. Acc.*, 2008, **120**, 215–241.
- S4 D. Jacquemin, E. A. Perpète, I. Ciofini, C. Adamo, R. Valero, Y. Zhao and D. G. Truhlar, *J. Chem. Theory Comput.*, 2010, **6**, 2071–2085.
- S5 D. Jacquemin, A. Planchat, C. Adamo and B. Mennucci, *J. Chem. Theory Comput.*, 2012, **8**, 2359–2372.
- S6 J. Tomasi, B. Mennucci and R. Cammi, *Chem. Rev.*, 2005, **105**, 2999– 3094.
- S7 R. Cammi, S. Corni, B. Mennucci and J. Tomasi, *J. Chem. Phys.*, 2005, **122**, 104513.
- S8 M. Caricato, B. Mennucci, J. Tomasi, F. Ingrosso, R. Cammi, S. Corni and G. Scalmani, *J. Chem. Phys.*, 2006, **124**, 124520.
- S9 F. Santoro, R. Improta, A. Lami, J. Bloino and V. Barone, *J. Chem. Phys.*, 2007, **126**, 084509.
- S10 F. Santoro, R. Improta, A. Lami, J. Bloino and V. Barone, *J. Chem. Phys.*, 2007, **126**, 184102.
- S11 F. Santoro, V. Barone and R. Improta, *J. Comput. Chem.*, 2008, **29**, 957–964